International Journal of Pharmaceutics 644 (2023) 123304

Contents lists available at ScienceDirect

International Journal of Pharmaceutics

journal homepage: www.elsevier.com/locate/ijpharm

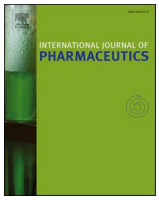

Chain length impact on the retro Diels-Alder mediated release of gemcitabine from hybrid nanoparticles towards pancreatic cancer therapy

Adeolu Oluwasanmi [a], Sarah Lindsay [b], Anthony Curtis [c], Yvonne Perrie [b], Clare Hoskins [a,*]

[a] Department of Pure and Applied Chemistry, University of Strathclyde, Glasgow G1 1RD, UK
[b] Strathclyde Institute of Pharmacy and Biomedical Sciences, University of Strathclyde, Glasgow G4 0RE, UK
[c] School of Pharmacy and Bioengineering, Keele University, Keele ST5 5BG, UK

ARTICLE INFO

Keywords:
Retro Diels-Alder
Gemcitabine
Pancreatic cancer
Hybrid nanoparticle
Thermo responsive drug delivery

ABSTRACT

Previously reported gold coated iron oxide nanoparticles (Au-IONP's) have demonstrated their effectiveness as drug delivery vehicles for gemcitabine conjugated to a thermally labile Diels-Alder linker containing a chain of 4 carbon atoms (TTLD4) for the treatment of pancreatic cancer. Heat generated via laser irradiation of Au-IONPs facilitated retro Diels-Alder mediated release in a burst release profile where approximately half of all total release over 180 min occurred within the first 5 min. Two analogues of TTLD4, which differ only in linker chain length (TTLD3 & TTLD6) were synthesised and conjugated to Au-IONP's. Heat-mediated release of gemcitabine at 45 °C over 180 min from these formulations was confirmed to be based on linker length, which was 94%, 76% and 45% for TTLD3, TTLD4 and TTLD6, respectively. Drug loading of the Diels-Alder linkers in a 5:1 Drug/Au-IONP w/w ratio appears to favour those containing an even number of carbons TTLD4 (76%) & TTLD6 (57%) over TTLD3 (25%), possibly due to the linker likely being positioned perpendicular to the Au-IONP surface because of the 120 °C–C bond.

1. Introduction

Pancreatic adenocarcinoma (pancreatic cancer) had a 5-year survival rate of approximately 4% in between 1971 and 2011 where no significant improvements in survival rates occurred ("Pancreatic cancer survival statistics | Cancer Research UK"). Within the same period, breast cancer 5-year survival rates were successfully improved from 52% to 87% ("Breast cancer survival statistics | Cancer Research UK"). In 2019, approximately 3% of all cancers are pancreatic cancer making it the 10th most common type of cancer, where the majority of diagnosed patients are 60+ years old. At the same time, it is responsible for 6% of all cancer related deaths, disproportionately making it the fifth most common cause of cancer related deaths. These statistics highlight the poor prognosis and lack of significant improvements in patient outcomes over the last 50 years. Surgical intervention (Whipples' procedure) is the only true method of ensuring full remission of treated patients and is often accompanied with post-surgical chemotherapy (Brooks and Culebras, 1976; Changazi et al., 2020; Nießen and Hackert, 2021). Only 20% of patients are able to have this life-saving surgery with the remaining left to focus on life-extension and symptom-mediating treatments alone (Konstantinidis et al., 2013; Latenstein et al., 2020). Several factors including the advanced age of most patients (70 years+), the need for highly invasive surgical resection, pre- and post-surgical chemotherapy, and a lack of symptoms prior to Stage 4 disease, all contribute to the abysmal 5-year survival rate, where over 80% of patients die within 12 months. Pancreatic cancer tumours are also surrounded by an extremely dense stroma of cells that reduces the uptake of chemotherapeutic agents within the tumour site (Karagiannis et al., 2012; Karamitopoulou, 2019; Ottaviano et al., 2006). Fibroblasts are a key component of the tumour stroma and may consist of 90% of the total tumour mass. They promote cancer growth, contributing to a reduced immune response, and aid in the invasion of tumour cells to new environments in late-stage cancer (Karagiannis et al., 2012). These cancer cells are also capable of producing collagens and their location within the pancreas provides access to insulin which makes the tumour microenvironment extremely suited for cancer cells to thrive, proliferate, and mutate into a metastatic form (Bachem et al., 2005).

There are several chemotherapeutic options when treating pancreatic cancer. These include, oxaliplatin, cisplatin, paclitaxel, irinotecan, 5-fluorouracil, capecitabine and gemcitabine (Conroy et al., 2018; Jameson et al., 2020). Often these are administered as stand-alone treatments such as gemcitabine or used in combination therapy such

* Corresponding author.
E-mail address: clare.hoskins@strath.ac.uk (C. Hoskins).

https://doi.org/10.1016/j.ijpharm.2023.123304
Received 6 March 2023; Received in revised form 8 August 2023; Accepted 9 August 2023
Available online 10 August 2023

as GemCap (gemcitabine & capecitabine) and nab-paclitaxel with gemcitabine (de Jong et al., 2022; Herrmann et al., 2007; Vreeland et al., 2019; Zhang et al., 2019). Combination therapies display improved activity but often come with new and more severe symptoms such as higher rates of neuropathy with nab-paclitaxel plus gemcitabine(von Hoff et al., 2013), and increased neutropenia, thrombocytopenia, and anaemia with the addition of veliparib with gemcitabine and cisplatin (O'Reilly et al., 2020), invalidating their use with some patients. This is due to the systemic side effects these chemotherapy drugs have, which indiscriminately damage both cancerous and healthy cells within the body leading to hair loss, nausea, and fatigue. Gemcitabine is a pyrimidine antimetabolite-based treatment for pancreatic cancer which has been shown to be effective in only 23.8% of patients (Burris et al., 1997). Historically, 5-FU treated patients had a 1-year survival rate of 2%, which was improved to 18% with the use of gemcitabine, establishing it as first-line treatment (Burris et al., 1997). Research efforts over the last 50 years have failed to significantly improve the 5-year survival rate ("Pancreatic cancer survival statistics | Cancer Research UK"). To improve long term patient outcomes, it is important to tackle the diagnosis and treatment of pancreatic cancer with novel strategies designed to counter the numerous difficulties of treating this deadly malignancy with gemcitabine. Gemcitabine is a small molecule with rapid renal clearance (Peters et al., 2007). As a result, the high doses required for effective activity may lead to hepatic and renal toxicity. Pancreatic cancer is virtually symptomless in the initial stages when treatment would be most effective with surgical resection being a viable option. A dense stroma acts as an effective barrier to chemotherapeutic agents including gemcitabine, partially due to counteracting the enhanced permeability and retention effect (EPR) which can be used to passively target tumours (Xie et al., 2020). The extracellular matrix within these tumour environments possesses a positive intratumoral pressure reducing permeability further (Xie et al., 2020).

Ensuring significant improvements in the treatment of pancreatic cancer with gemcitabine requires a method to bypass the low permeability of the tumour environment, the rapid clearance of gemcitabine after administration, preventing or reducing systemic side effects and providing a means of early diagnosis. Oluwasanmi *et al.* previously designed a novel drug formulation for the treatment of pancreatic cancer (Oluwasanmi et al., 2017). This thiolated thermally labile drug (TTLD4) formulation is comprised of a gemcitabine molecule covalently conjugated to the surface of gold coated iron oxide hybrid nanoparticles (Au-IONP's) *via* a thermally labile Diels-Alder linker that contains a chain comprising four carbon atoms. The iron oxide core of this formulation confers MRI imaging properties, and the gold coating improves bioavailability, prevents iron leeching, and provides a source of heat generation via its surface plasmon resonance property after exposure to near infra-red radiation (Yang et al., 2021). The Au-IONP's are taken up by a combination of passive and energy dependant endocytosis and are retained intracellularly, allowing for their accumulation over time and making them effective drug delivery vehicles (Barnett et al., 2013). Retro Diels-Alder mediated drug release of approximately 80% was observed over 60 sec at 44 °C in a "burst release" profile with near-total release occurring after 30 min. At 37 °C, this burst release window resulted in a release of only 14%, a 5-fold reduction over an 8 °C temperature range. At 5 and 20 °C, less than 0.5% release was observed over a 4-week period displaying the drug formulation's stability under normal storage conditions. Overall, studies with murine pancreatic xenograft models demonstrated a 62% reduction in tumour weight with this formulation compared to locally administered free gemcitabine after laser irradiation (Oluwasanmi et al., 2017).

The Diels-Alder reaction was first described and published by Otto Diels and Kurt Alder in 1928 which earned them the Nobel Prize in Chemistry (Diels and Alder, 1929). It is a reversible reaction between a conjugated diene and a dienophile forming a cyclohexane, which undergoes the retro Diels-Alder reaction at elevated temperatures (Borsenberger and Howorka, 2009; Qiu, 2015; Rickborn, 1998; Zhou et al., 2012). It is widely accepted that the Diels-Alder reaction proceeds under a single concerted step via a cyclic transition state (Houk et al., 1986). All atoms and electrons are conserved in the forward and reverse reaction making it an especially useful click-chemistry process. This is a valuable attribute to exploit in pharmaceutical applications due to the lack of side products (Kolb et al., 2001).

The simplest example of the Diels-Alder reaction is between ethene and 1,3-butadiene to produce cyclohexene. The Diels-Alder reaction can be promoted or hindered depending on the substituents present on the diene and dienophile (Boutelle and Northrop, 2011). Electron withdrawing groups bonded to the sp2 carbon of dienophiles, such as the carbonyl groups in maleimide, promote the formation of the Diels-Alder cycloadduct, as do electron donating groups on the diene. In general, the cycloadduct formation can be described as endergonic (retro Diels-Alder favoured, Diels-Alder hindered), reversible or exergonic (Diels-Alder favoured, retro Diels-Alder hindered). Substituent effects on the dienophile have been stated to have low significance on reaction kinetics when compared to the diene, which depending on the substituent can form irreversible cycloadducts (Boutelle and Northrop, 2011). The free energies (ΔG) for the Diels-Alder reaction between furan and maleimide are −1.2 and −3.3 kcal/mol for the endo and exo isomer, respectively, confirming the reaction's reversible and slightly exergonic status. The reaction is more exergonic between furan and N-methylmaleimide (−3.0 and −4.5 kcal/mol for the endo and exo isomer), meaning that the retro Diels-Alder reaction would be more hindered. The literature lacks further information regarding the impact of alkyl chain length of N-alkylmaleimides on the retro Diels-Alder energy requirements.

We hypothesised that drug release would directly correlate with linker length, where shorter linkers led to faster release rates via the temperature mediated retro Diels-Alder reaction. Theoretically this would be due to fewer steric effects experienced by the smaller compounds as they migrate away from the surface. Drug loading may directly correlate with linker length where shorter linkers experience less steric hinderance promoting higher surface attachment. However, the orientation of the TTLD linkers themselves on the surface could be affected by how linear the linkers are, where an even number of alkyl carbons, which promotes linearity could improve drug loading efficiency.

In this study the effects of TTLD's linker chain length on release properties from the Au-IONP surface were investigated to determine optimum formulation strategy. By utilizing three synthetically derived maleimide-esters of different alkyl chain lengths (3, 4 and 6 carbon atoms) various TTLD linkers were prepared as shown in Fig. 1. Drug loading and retro Diels-Alder mediated drug release was performed to determine the effect of linker chain length on these properties.

2. Materials and methods

Gemcitabine HCl, maleic anhydride, *N*-hydroxysuccinimide, *N*-(3-dimethylaminopropyl)-*N'*-ethylcarbodiimide (EDCI), and Di-*tert*-butyl dicarbonate (Boc anhydride) were purchased from Fluorochem UK Ltd. βalanine, γ-aminobutyric acid, 6-aminocaproic acid, 2-furanmethanethiol, ethyl acetate, trifluoroacetic acid (TFA), gold chloride, hydroxylamine, iron sulphate heptahydrate, celite, and *N,N*-dimethylformamide (DMF) were purchased from Merck Ltd. Chloroform, dichloromethane, methanol, acetonitrile, 1,4-dioxane and diisopropylethylamine (DIPEA) were purchased from Fisher Scientific. Flash chromatography was performed using 40–63 μm silica gel (60 Å, 230–400 mesh) conditioned with the appropriate chilled solvent prior to loading and elution. Optimal solvent systems for purification were determined with the use of thin layer chromatography (TLC) with various solvent ratios, which are shown in Table S1-14 within the supplementary info. Rotary evaporation of intermediates was performed at 5 °C unless otherwise stated. All intermediates and the final linkers were stored at −20 °C. ^{1}H NMR was conducted on a Bruker AVIII-HD-500 NMR Spectrometer with TMS (^{1}H: $\delta = 0.00$ ppm) and 2,3,5,6-tetrachloronitrobenzene as a reference

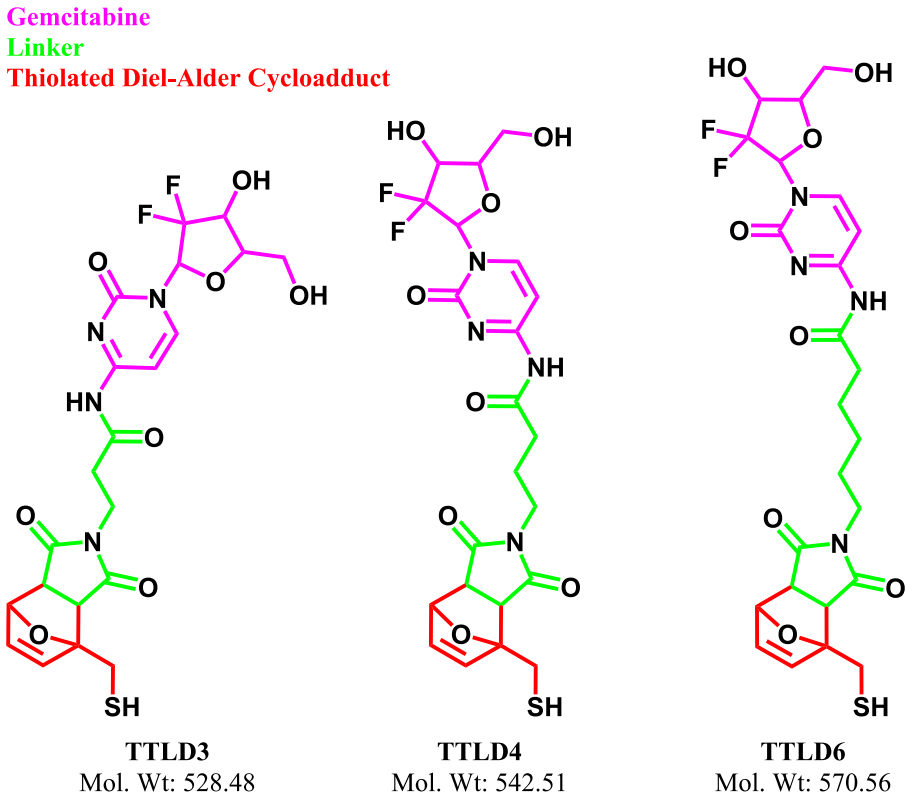

Fig. 1. Chemical structure of 3, 4 and 6 length TTLD linkers attached to gemcitabine.

and analytical standards, respectively.

Synthesis of the different TTLD analogues, described in the scheme in Fig. 2A-C, was achieved by the use of amino acid analogues (compound 2) containing different chain lengths. These intermediates were subsequently used in the synthesis of the three TTLD linkers described as, (TTLD3, chain containing 3 carbons), (TTLD4, chain containing 4 carbons) or (TTLD6, chain containing 6 carbons), which are initially derived from 3-maleimidopropionic acid N-hydroxysuccinimide ester, 4-maleimidobutyric acid N-hydroxysuccinimide ester, and 6-maleimidohexanoic acid N-hydroxysuccinimide ester, respectively.

2.1. Route synthetic procedures for TTLD3, TTLD4 and TTLD6

2.1.1. Synthesis of 3-maleimidopropionic acid N-hydroxysuccinimide ester (4a)

Maleic anhydride (4.0 g, 41 mmol) and β-alanine (4.0 g, 45 mmol) were dissolved in anhydrous DMF (48 mL) and stirred under nitrogen at room temperature for 3 h. The mixture was then cooled to 0 °C for 30 min before the addition of *N*-hydroxysuccinimide (5.36 g, 47 mmol) followed by EDCI (16.06 g, 103 mmol). The temperature was maintained at 0 ℃ for a further 30 min, before being allowed to slowly reach room temperature and stirred overnight under nitrogen. The mixture was concentrated *in vacuo* at 40 ℃, dissolved in chloroform (400 mL) and washed with saturated sodium bicarbonate (135 mL). The organic layer was dried with magnesium sulphate, filtered, and concentrated *in vacuo* at 40 °C to yield 19.5 g of a crude brown powder. The crude material was purified by column chromatography (Table S1) to yield the ester as a white powder (7.5 g, 74% recovery, 69 % overall yield) (Song et al., 2009). RF (by TLC) = 0.20 (chloroform - methanol 95:5). ^{1}H NMR: δ 7.02 (s, 2H), 3.77 (t, 2H), 3.05 (t, 2H), 2.81 (s, 4H).

2.1.2. Synthesis of 4-maleimidobutyric acid N-hydroxysuccinimide ester (4b)

Maleic anhydride (4.0 g, 41 mmol) and γ-aminobutyric acid (4.63 g, 45 mmol) were dissolved in anhydrous DMF (48 mL) and stirred under nitrogen at room temperature for 3 h. The mixture was then cooled to 0 °C for 30 min before the addition of *N*-hydroxysuccinimide (5.36 g, 47 mmol) followed by EDCI (16.06 g, 103 mmol). The temperature was maintained at 0 °C for a further 30 min, before being allowed to slowly reach room temperature and stirred overnight under nitrogen. The mixture was concentrated *in vacuo* at 40 °C, dissolved in chloroform (400 mL) and washed with saturated sodium bicarbonate (135 mL). The organic layer was dried with magnesium sulphate, filtered, and concentrated *in vacuo* at 40 °C to yield 14.6 g of a dark green sticky solid. The crude material was purified by column chromatography (Table S2) to yield the ester as a white powder (8.5 g, 80% recovery, 74% overall yield) (Song et al., 2009). RF (by TLC) = 0.29 (chloroform - methanol 9:1) ^{1}H NMR: δ 6.99 (s, 2H), 3.51 (t, 2H), 2.82 (s, 4H), 2.73 (t, 2H), 1.87 (t, 2H).

2.1.3. Synthesis of 6-maleimidohexanoic acid N-hydroxysuccinimide ester (4c)

Maleic anhydride (4.0 g, 41 mmol) and 6-aminocaproic acid (5.89 g, 45 mmol) was dissolved in anhydrous DMF (48 mL) and stirred under nitrogen at room temperature for 3 h. The mixture was then cooled to 0 °C for 30 min before the addition of N-hydroxysuccinimide (5.36 g, 47 mmol) followed by EDCI (16.06 g, 103 mmol). The temperature was maintained at 0 °C for a further 30 min, before being allowed to slowly reach room temperature and stirred overnight under nitrogen. The mixture was concentrated *in vacuo* at 40 °C, dissolved in chloroform (400 mL) and washed with saturated sodium bicarbonate (135 mL). The organic layer was dried with magnesium sulphate, filtered, and concentrated *in vacuo* at 40 °C to yield 12.9 g of a highly viscous yellow oil of 12.9 g (10.2 g, 79% pure, 81% yield assay corrected by ^{1}H NMR). The crude material was purified by column chromatography (Table S3) to yield the ester as a white powder (9.0 g, 88% recovery, 72% overall yield) (Song et al., 2009). RF (by TLC) = 0.13 (chloroform - methanol 97:3) ^{1}H NMR: δ 7.00 (s, 2H), 3.40 (t, 2H), 2.82 (s, 4H), 2.65 (t, 2H), 1.64

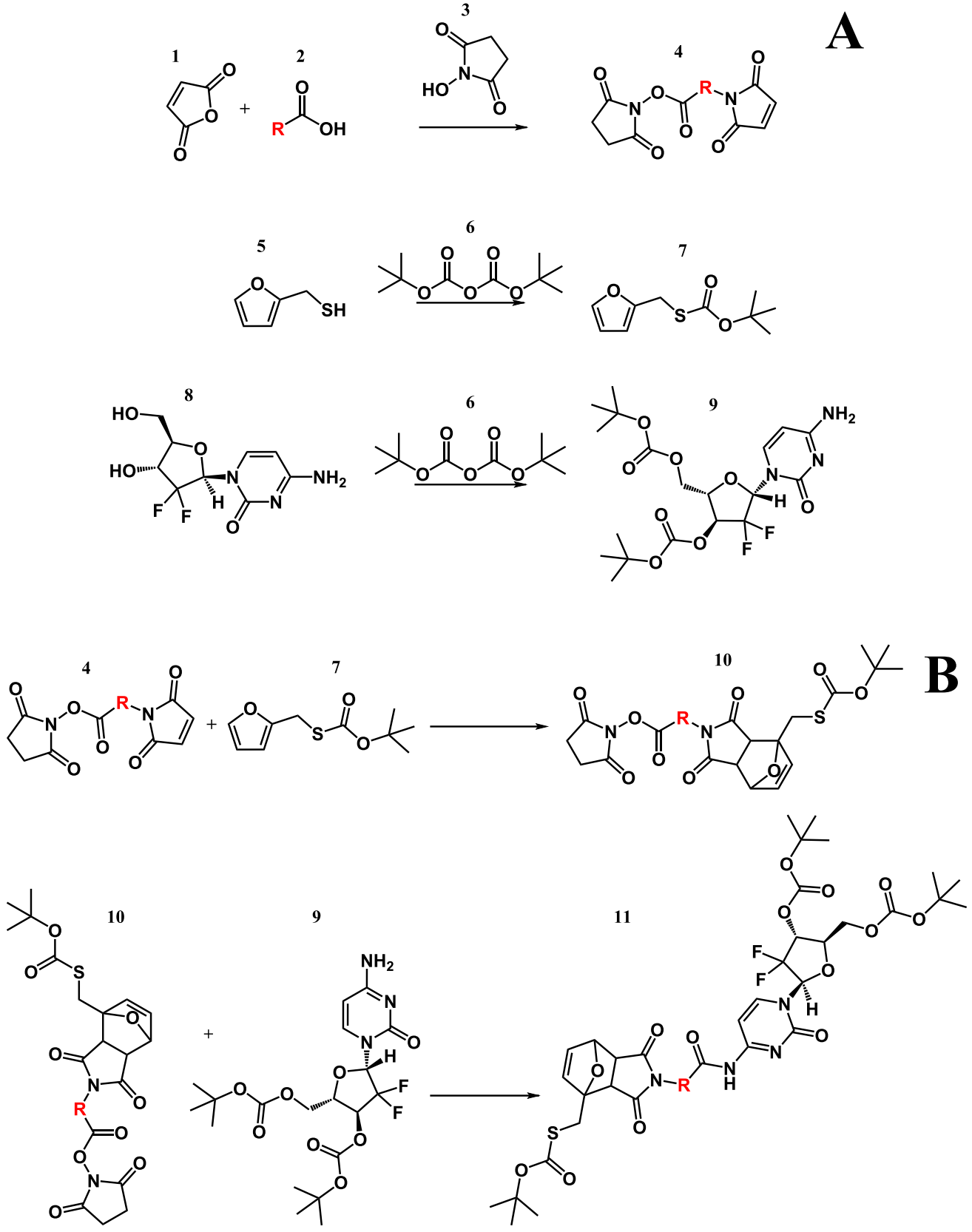

Fig. 2. (A–C) Reaction scheme for the synthesis of TTLD3 (R1), TTLD4 (R2) and TTLD6 (R3).

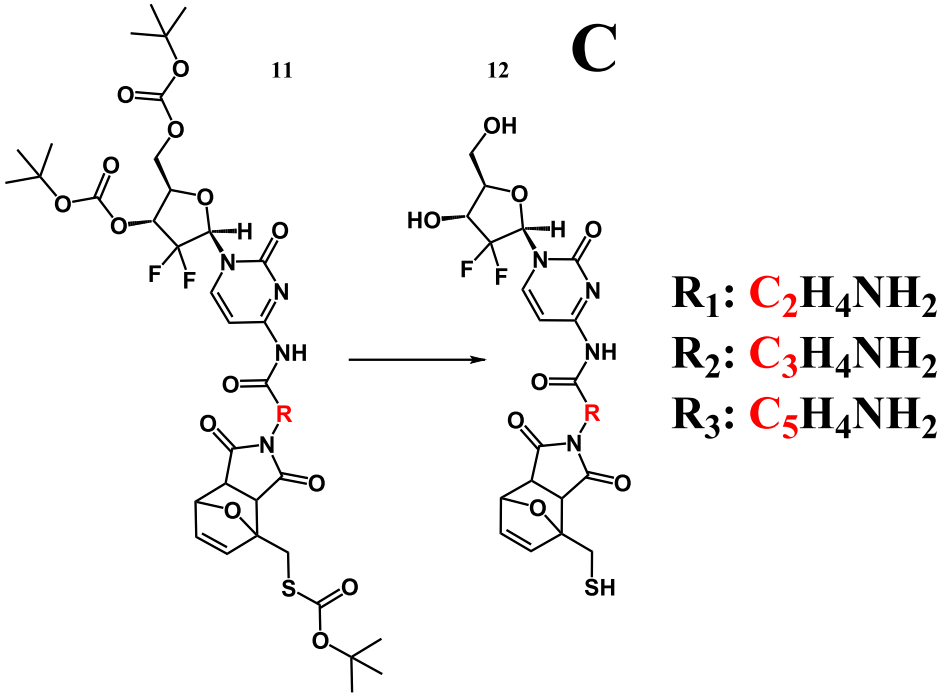

Fig. 2. (*continued*).

(m, 2H), 1.53 (m, 2H), 1.32 (m, 2H).

2.1.4. Synthesis of O-tert-butyl S-(furan-2-ylmethyl) carbonothionate (6)

Boc anhydride (19.12 g, 88 mmol) and 2-furanmethanethiol (10.0 g, 88 mmol) were dissolved in anhydrous acetonitrile (350 mL) and stirred at room temperature. Potassium carbonate (24.21 g, 175 mmol) was added, and the mixture was stirred at room temperature under nitrogen for 24 h. The mixture was diluted with ethyl acetate (2 L) and filtered through a celite pad. The filtrate was washed with saturated sodium bicarbonate (400 mL), dried with magnesium sulphate, and filtered. The filtrate was concentrated *in vacuo* at 40 ℃ to yield *O-tert*-butyl *S*-(furan-2-ylmethyl) carbonothionate as a brown oil of 18.3 g (17.5 g, 95% pure, 93% yield assay corrected) which was used without further purification (Temperini et al., 2010). RF (by TLC) = 0.36 (pet ether 100%) ^{1}H NMR: δ 7.32 (s, 1H), 6.29 (s, 1H), 6.23 (s, 1H), 4.05 (s, 2H), 1.50 (s, 9H).

2.1.5. Synthesis of Boc protected 3-Carbon linker (7a)

Chilled dichloromethane (50 mL) was charged into a sealed tube followed by the addition of *O-tert*-butyl *S*-(furan-2-ylmethyl) carbonothionate (5.0 g, 23.3 mmol) and 3-maleimidopropionic acid *N*-hydroxysuccinimide ester (4a) (6.21 g, 23.3 mmol). The mixture was stirred at room temperature under a nitrogen atmosphere for 7 days, and the reaction was monitored by ^{1}H NMR. The mixture was concentrated *in vacuo* at 5 ℃. The Boc-protected 3-carbon linker (3-BDA) was obtained as 11.9 g of a crude brown solid. Purification by column chromatography (Table S4) yielded Boc-protected 3-carbon linker (3-BDA) as an off-white powder (4.9 g, 72% recovery, 44% overall yield). RF (by TLC) = 0.46 (pet ether - ethyl acetate 4:1) ^{1}H NMR: δ 6.52–6.44 (s, 1H, endo/exo), 6.39–6.31(s, 1H, endo/exo), 5.23 (t, 1H), 3.73 (t, 2H), 3.80, 3.59 (s, 1H, endo/exo), 3.44, 3.06 (s, 1H, endo/exo) 2.99 (t, 2H), 2.82 (s, 4H), 1.50 (s, 9H).

2.1.6. Synthesis of Boc protected 4-Carbon linker (7b)

Chilled dichloromethane (50 mL) was charged into a sealed tube followed by the addition of *O-tert*-butyl *S*-(furan-2-ylmethyl) carbonothionate (5.0 g, 23.3 mmol) and 4-maleimidobutyric acid *N*-hydroxysuccinimide ester (4b) (6.54 g, 23.3 mmol). The mixture was stirred at room temperature under a nitrogen atmosphere for 7 days, and the reaction was monitored by ^{1}H NMR. The mixture was concentrated *in vacuo* at 5 ℃. The Boc protected 4-carbon linker (4-BDA) was obtained as 13.7 g of a brown gum. Purification by column chromatography (Table S5) yielded Boc-protected 4-carbon linker (4-BDA) as a white powder (6.4 g, 68% recovery, 55% overall yield). RF (by TLC) = 0.28 (pet ether - ethyl acetate 9:1) ^{1}H NMR: δ 6.53–6.45 (s, 1H, endo/exo), 6.40–6.31(s, 1H, endo/exo), 5.23 (t, 1H), 3.81, 3.70 (s, 1H, endo/exo), 3.58 (t, 2H), 3.01, 2.95 (s, 1H, endo/exo) 2.83 (s, 4H), 2.02 (m, 2H), 1.90 (m, 2H), 1.50 (s, 9H).

2.1.7. Synthesis of Boc protected 6-carbon linker (7c)

Chilled dichloromethane (50 mL) was charged into a sealed tube followed by the addition of *O-tert*-butyl *S*-(furan-2-ylmethyl) carbonothionate (5.0 g, 23.3 mmol) and 6-maleimidohexanonic acid *N*-hydroxysuccinimide ester (4c) (7.19 g, 23.3 mmol). The mixture was stirred at room temperature under a nitrogen atmosphere for 7 days, and the reaction was monitored by ^{1}H NMR. The mixture was concentrated *in vacuo* at 5 ℃. The Boc protected 6-carbon linker (6-BDA) was obtained as 14.7 g of a brown oil. Purification by column chromatography (Table S6) yielded Boc-protected 6-carbon linker (6-BDA) as an off-white powder (6.8 g, 79% recovery, 56% overall yield). RF (by TLC) = 0.33 (pet ether - ethyl acetate 4:1) ^{1}H NMR: δ 6.51–6.40 (s, 1H, endo/exo), 6.40–6.29 (s, 1H, endo/exo), 5.21 (t, 1H), 3.81, 2.98 (s, 1H, endo/exo), 3.67, 2.91 (s, 1H, endo/exo), 3.49 (t, 2H), 3.42, 3.31 (s, 1H, endo/exo) 2.83 (s, 4H), 2.59 (t, 2H), 1.76 (m, 2H), 1.61 (m, 2H), 1.51 (s, 9H), 1.39 (m, 2H).

2.1.8. Synthesis of 3′,5′-O-bis(tert-Butoxycarbonyl)gemcitabine (9)

Boc anhydride (72.83 g, 0.33 mol) was dissolved in 1,4-dioxane (665 mL) and the solution was added dropwise to a stirred solution of gemcitabine HCl (10.0 g, 33 mmol) in 1 M aqueous potassium hydroxide (665 mL) over 10 min at room temperature. The mixture was closely monitored by TLC (1:1 acetone/dichloromethane) to observe the appearance of a spot at Rf 0.25 corresponding to a mono-Boc-protected gemcitabine. The reaction was worked up when the mono-Boc-protected gemcitabine and gemcitabine (Rf 0.05) were present in an apparent 1:1 ratio. The mixture was extracted with ethyl acetate (1330 mL), washed with brine (330 mL), and dried with magnesium sulphate. The mixture

was filtered and concentrated *in vacuo* at 40 ℃ yielding a clear oily residue. The oily residue was dissolved in 1,4-dioxane (665 mL), followed by the addition of Boc anhydride (72.83 g, 0.33 mol) as a solution in 1 M aqueous potassium hydroxide (665 mL). The mixture was stirred at room temperature and monitored closely by TLC, which typically showed a spot at Rf 0.45 for the di-Boc-protected product, a faint spot for the tri-Boc-protected impurity (Rf 0.9) and the disappearance of the spot corresponding to the mono-Boc-protected intermediate. The reaction was worked-up immediately if the spot corresponding to the tri-Boc-protected impurity increased in size and darkened. The mixture was extracted with ethyl acetate (1330 mL), washed with brine (330 mL), and dried with magnesium sulphate. The mixture was filtered and concentrated *in vacuo* at 5 ℃ to yield 33.7 g of a pale-yellow oily residue. Purification by column chromatography (Table S7) yielded a white solid (12.3 g, 83% recovery, 80% overall yield) (Guo and Gallo, 1999). RF (by TLC) = 0.26 (Dichloromethane (DCM) - acetone 9:1) ^{1}H NMR: δ 7.59 (d, 1H), 6.40 (br, 1H), 6.01 (d, 1H), 5.28 (br, 1H), 4.52 – 4.43 (m, 3H), 1.50 (s, 18H).

2.1.9. Coupling of the Boc-protected 3-carbon linker (7a) with 3′,5′-O-Bis (tert-Butoxycarbonyl)gemcitabine (9) to give Boc-protected conjugate (10a)

3′,5′-O-Bis(*tert*-Butoxycarbonyl)gemcitabine (4.00 g, 8.6 mmol) was dissolved in chilled anhydrous dichloromethane (32 mL) and stirred under nitrogen. Boc-protected 3-carbon linker (7a) (4.15 g, 8.6 mmol) was added, followed by DIPEA (7.52 mL, 43 mmol) and the mixture was stirred at 5 ℃ under nitrogen for 7 days under a nitrogen atmosphere. The reaction was monitored by ^{1}H NMR. The mixture was concentrated *in vacuo* at 5 ℃. Purification by column chromatography yielded 8.4 g of the Boc protected 3-carbon thermally labile drug-linker conjugate (10a) (3-Boc-TTLD) as a brown solid. Further purification by column chromatography (Table S8) yielded the conjugate (10a) as an off-white solid (3.8 g, 81% recovery, 53% overall yield). RF (by TLC) = 0.10 (pet ether - ethyl acetate 9:1) ^{1}H NMR: δ 7.89 (d, 1H), 7.25 (d, 1H), 6.46, 6.26 (m, 2H, endo/exo), 5.18 (br, 1H), 4.95 (s, 1H), 4.36 (m, 3H). 3.67 (m, 2H), 3.58, 2.97 (s, 1H, endo/exo), 3.52, 2.88 (s, 1H, endo/exo), 3.44 (m, 2H), 1.35 (s, 27H).

2.1.10. Coupling of the Boc-protected 4-carbon linker (7b) with 3′,5′-O-bis (tert-Butoxycarbonyl)gemcitabine (9) to give Boc-protected conjugate (10b)

3′,5′-O-Bis(*tert*-Butoxycarbonyl)gemcitabine (4.00 g, 8.6 mmol) was dissolved in chilled anhydrous dichloromethane (32 mL) and stirred under nitrogen. Boc-protected 4-carbon linker (7b) (4.27 g, 8.6 mmol) was added, followed by DIPEA (7.52 mL, 43 mmol) and the mixture was stirred at 5 ℃ under nitrogen for 7 days under a nitrogen atmosphere. The reaction was monitored by ^{1}H NMR. The mixture was concentrated *in vacuo* at 5 ℃. Purification by column chromatography (Table S9) yielded 8.4 g of the Boc protected 4-carbon thermally labile drug-linker conjugate (10b) (4-Boc-TTLD) as a brown solid. Further purification by column chromatography yielded the conjugate (10b) as a green solid (3.1 g, 58% recovery, 43% overall yield). RF (by TLC) = 0.07 (pet ether - ethyl acetate 9:1) ^{1}H NMR: δ 7.89 (d, 1H), 7.45 (d, 1H), 6.62, 6.41 (m, 1H, endo/exo), 6.60, 6.41 (m, 1H, endo/exo), 5.34 (br, 1H), 5.25, 5.14 (s, 1H, endo/exo), 4.56–4.51 (m, 3H). 3.59, 3.14 (m, 1H, endo/exo), 3.56 (t, 2H) 3.39 (t, 2H), 3.39, 3.03 (s, 1H, endo/exo), 2.60 (m, 2H,), 1.93 (m, 2H), 1.51 (s, 27H).

2.1.11. Coupling of the Boc-protected 6-carbon linker (7c) with 3′,5′-O-bis (tert-Butoxycarbonyl)gemcitabine (9) to give Boc-protected conjugate (10c)

3′,5′-O-Bis(*tert*-Butoxycarbonyl)gemcitabine (4.00 g, 8.6 mmol) was dissolved in chilled anhydrous dichloromethane (32 mL) and stirred under nitrogen. Boc-protected 6-carbon linker (7c) (4.51 g, 8.6 mmol) was added, followed by DIPEA (7.52 mL, 43 mmol) and the mixture was stirred at 5 ℃ under nitrogen for 7 days under a nitrogen atmosphere. The reaction was monitored by ^{1}H NMR. The mixture was concentrated *in vacuo* at 5 ℃. Purification by column chromatography (Table S10) yielded 9.4 g of the Boc protected 6-carbon thermally labile drug-linker conjugate (10c) (6-Boc-TTLD) as a deep brown solid. Further purification by column chromatography yielded the conjugate (10c) as a pale orange solid (3.4 g, 73% recovery, 45% overall yield). RF (by TLC) = 0.13 (pet ether - ethyl acetate 9:1) ^{1}H NMR: δ 7.99 (d, 1H), 7.45 (d, 1H), 6.61, 6.40 (m, 1H, endo/exo), 6.46, 6.40 (m, 1H, endo/exo), 5.32 (br, 1H), 4.60–4.35 (m, 3H). 3.82, 3.09 (m, 1H, endo/exo), 3.45, 3.02 (m, 1H, endo/exo), 3.46 (t, 2H), 2.56 (m, 2H), 1.71 (m, 2H,), 1.59 (m, 2H), 1.51 (s, 27H), 1.36 (m, 2H).

2.1.12. Deprotection of 3-Boc-TTLD to give conjugated gemcitabine TTLD3 (11a)

The previously synthesised 3-Boc-TTLD (10a) (3.5 g, 4.2 mmol) was dissolved in a cold solution of 15% v/v% of TFA:DCM (140 mL) and stirred for 2 h at 0 ℃. The mixture was concentrated *in vacuo* at 5 ℃ to give 3.1 g of a deep red viscous solid. Purification by column chromatography (Table S11) yielded TTLD3 (11a) (0.71 g, 32% yield). RF (by TLC) = 0.28 (DCM - methanol 95:5) ^{1}H NMR: δ 8.38 (d, 1H), 7.38 (d, 1H), 6.50, 6.28 (s, 1H, endo/exo), 6.40, 6.28 (s, 1H, endo/exo), 5.25, 5.13 (s, 1H, endo/exo), 4.49 (br, 1H), 4.05 (m, 4H). 3.91 (m, 3H), 3.91, 3.13, 3.08 (m, 2H, endo/exo), 2.24 (s, 1H). ESI MS *m/z* 527 [negative, (M – H)].

2.1.13. Deprotection of 4-Boc-TTLD to give conjugated gemcitabine TTLD4 (11b)

The previously synthesised 4-Boc-TTLD (10b) (2.8 g, 3.3 mmol) was dissolved in a cold solution of 15% v/v% of TFA:DCM (112 mL) and stirred for 2 h at 0 ℃. The mixture was concentrated *in vacuo* at 5 ℃ to give 2.5 g of a deep red viscous solid. Purification by column chromatography (Table S12) yielding TTLD4 (11b) (0.79 g, 44% yield). RF (by TLC) = 0.24 (DCM - methanol 95:5) ^{1}H NMR: δ 8.29 (d, 1H), 7.39 (d, 1H), 6.55, 6.29 (s, 1H, endo/exo), 6.45, 6.29 (s, 1H, endo/exo), 5.25, 5.15 (s, 1H, endo/exo), 4.48 (br, 1H), 4.04, 3.88 (m, 3H). 3.50, 3.10 (m, 1H, endo/exo), 3.35, 3.05 (m, 1H, endo/exo), 2.55 (m, 2H), 2.26 (s, 1H), 1.92 (t, 2H). ESI MS *m/z* 543 [negative, (M + H)].

2.1.14. Deprotection of 6-Boc-TTLD to give conjugated gemcitabine TTLD6 (11c)

The previously synthesised 6-Boc-TTLD (10c) (3.0 g, 3.4 mol) was dissolved in a cold solution of 15% v/v% of TFA:DCM (120 mL) and stirred for 2 h at 0 ℃. The mixture was concentrated *in vacuo* at 5 ℃ to give 2.6 g of a deep red viscous solid. Purification by column chromatography (Table S13) yielding TTLD6 (11c) (0.57 g, 29% yield). RF (by TLC) = 0.18 (DCM - methanol 95:5) ^{1}H NMR: δ 8.15 (d, 1H), 7.26 (d, 1H), 6.48, 6.32 (s, 1H, endo/exo), 6.27, 6.15 (s, 1H, endo/exo), 5.08, 4.98 (s, 1H, endo/exo), 4.34 (br, 1H), 3.89, (m, 2H). 3.75 (m, 1H), 3.62, 3.43 (m, 1H, endo/exo), 3.43 (t, 2H), 3.31 (m, 1H, endo/exo), 2.41 (t, 2H), 1.56 (m, 2H), 1.44 (m, 2H), 1.20 (m, 2H). ESI MS *m/z* 571 [positive, (M + H)].

2.2. Synthesis of gold coated iron oxide nanoparticles

All glassware was previously treated with aqua regia and thoroughly rinsed with deionised (DI) water prior to use. Au-IONP's were synthesised with previously reported procedures (Barnett et al., 2013, n.d.; Hoskins et al., 2012; Oluwasanmi et al., 2017). The resultant Au-IONP's were analysed with an Agilent Technologies 700 series inductive coupled plasma – optical emission spectroscopy (ICP-OES) to determine metal content, and a Jeol Jem-1230 transmission electron microscopy (TEM) for size determination. Throughout the procedure, the particles were analysed for their zeta potential (ZP) and their size and size distribution with dynamic light scattering (DLS), with both ZP and DLS measurements performed with a Malvern Zetasizer Nano ZS.

2.3. ICP-OES sample preparation of Au-IONP's

A 100 μL aliquot of neat Au-IONP stock was mixed with gentle

heating in a 1:1 mixture of nitric acid and hydrochloric acid (900 μL) to aid dissolution. Following this, a 100 μL aliquot of the dissolved Au-IONP acid mixture was transferred to 9.9 mL of DI water and analysed with an Agilent 700 Series ICP Optical Emission Spectrometer for iron and gold content with ICP-OES.

2.4. Drug loading of Au-IONP's

A 1 mg mL^{-1} suspension of Au-IONP's (15 mL) based on iron concentration, was loaded with 75 mg of the appropriate linker (5:1) and shaken for 2 h at 5 ℃. The Au-IONP's were magnetically separated, and the supernatant was collected. The Au-IONP's were suspended in 15 mL of DI water, shaken, and then magnetically separated to collect the supernatant. This was repeated a final time for a total of 3 × 15 mL supernatants, before the Au-IONP's were suspended in 15 mL of DI water and refrigerated for future use. The supernatants were then analysed with an Agilent Cary 60 UV–Vis Spectrophotometer and the combined mass of detected drug was used to determine the extend of drug loading.

2.5. Stability study and temperature driven drug release studies from Au-IONP's

DI water (1.2 mL) was charged into an Eppendorf tube followed by 400 μL of drug loaded Au-IONP's. This was performed in triplicate. The tubes were shaken well and placed into an Eppendorf heating block and heated to 37, 45 and 60 ℃. The tubes were sampled at specific intervals by magnetically settling the Au-IONP's, sampling the supernatants (100 μL) before shaking and returning the tubes back into the heating block. The samples were diluted with 900 μL DI water into high performance liquid chromatography (HPLC) vials and analysed by HPLC. Heat-mediated release was achieved with the use of thermal blocks housing the Eppendorf tubes. The drug release studies were performed at 37, 45 and 60 °C over a 3 h duration. In addition, a control experiment at 20 ℃ served as a stability study that was performed over 3 h.

3. Results and discussion

The Au-IONP's were successfully synthesised and characterised with ultraviolet–visible spectroscopy (UV–Vis), ZP, DLS, TEM and ICP-OES. The TTLD linkers were primarily characterized by ^{1}H NMR and drug loading and release was determined with HPLC analysis.

3.1. ^{1}H NMR spectrometry

Successful synthesis of the three linkers was determined by ^{1}H NMR and the spectral data for their intermediates are located in the supplementary info (Figs. S1-14).

3.2. Mass spectrometry

All three linkers were individually dissolved in acetonitrile (1 mg mL^{-1}) and analysed with a Thermo Scientific Vanquish HPLC-MS system. The mass spectra for TTLD3, TTLD4 and TTLD6 respectively are shown in Figs. S15-17 of the supplementary information.

3.3. UV–Vis spectroscopy of Au-IONP's

An aliquot of Au-IONP's were diluted and analysed with UV–Vis spectroscopy using an Agilent Cary 60 UV–Vis Spectrophotometer between 400 nm and 800 nm and compared with IONP's. IONP's absorb UV light across the 400–800 nm range that diminishes with increasing wavelength. The presence of the surface gold coat on the Au-IONP's facilitates absorbance in the 500–650 nm range indicating its presence as shown in Fig. S18 of the supplementary information (Barnett et al., 2012; Hoskins et al., 2012).

Table 1
Surface charge measurements of iron oxide nanoparticles and hybrid nanoparticles.

Particle	Metal Content analysis (μgmL-1)		Size from TEM (±SD)	Size from DLS (±SD)	Zeta Potential (mV) (±SD)
	Fe	Au			
IONP	–	–	97 (6)	450.1 (606.8)	−19.4 (0.7)
PEI-IONP	–	–	110 (21)	820.4 (102.3)	+41.0 (0.4)
Au(seed) PEI-IONP	–	–	98 (7)	1320 (138.1)	+28.3 (1.3)
HNP	1866	2477	94 (11)	625.1 (406.6)	+18.5 (0.3)

3.4. Zeta potential and DLS size measurements of Au-IONP's

The results of the DLS measurements for particle size and zeta potential measurements for surface charge is shown in Table 1. The surface charge of the Au-IONP's was 18.5 mV which is similar to established values in literature.(Barnett et al., 2012). The initial IONP's had a negative surface charge of −19.4 mV. Successful PEI coating was confirmed with the positive surface charge of 41 mV. Analysis of Au-IONP size by DLS is difficult due to the formation of aggregates that can occur mid analysis. TEM is a better suited means of determining true Au-IONP size.

3.5. Transmission emission microscopy of Au-IONP's

DLS measurements for particle size was problematic due to aggregation occurring during analysis. TEM imaging of the Au-IONP's shown in Fig. 3D confirmed their average size to be 90–120 nm. The gold seeds on the surface of the PEI-Coated IONP's are visible in Fig. 3C.

3.6. ICP-OES analysis of Au-IONP's

Metal content of the nanoparticle samples was quantified with the use of calibration line equations with an R^2 of 0.999 for both iron and gold, which were generated by the analysis of gold and iron standards with ICP-OES at a concentration range of 0.05 ppm to 10 ppm at 261.187 and 242.794 nm for iron and gold, respectively. The concentration of the Au-IONP's was determined to be 18.66 mg mL^{-1} and 24.77 mg mL^{-1} for iron and gold respectively (1:1.33).

3.7. Drug loading

After drug loading and washes via magnetic separation, the wash solutions were analysed by HPLC. The extent of drug loading and release was calculated using a calibration curve for the three TTLD analogues where the R^2 was 0.99997, 0.99998 and 0.99994 for TTLD3, TTLD4 and TTLD6, respectively. The intensity of the 3rd wash solution for each TTLD analogue was found to be less than 0.05 mg mL^{-1}, confirming that true drug loading was calculated to an accuracy of >1% of the 5 mg mL^{-1} TTLD used.

Overall, drug loading was observed to be 25.3, 76.1 and 56.7% for TTLD3, TTLD4 and TTLD6, respectively, as shown in Fig. 4A. This confirms that the extent of drug loading does not correlate to linker length, at least when considering these three relatively short chain lengths. Overall, the drug – Au-IONP concentration in each formulation was 1.27, 3.80 and 2.83 mg mL^{-1} drug per mg Au-IONP for TTLD3, TTLD4 and TTLD6, respectively as shown in in Fig. 4B.

This is likely due to the shorter TTLD3′s surface conjugation being limited due to potential steric hindrance of the bulkier gemcitabine group. The longer 6-carbon linker may be more flexible causing the molecule to lie horizontally on the Au-IONP surface, giving rise to

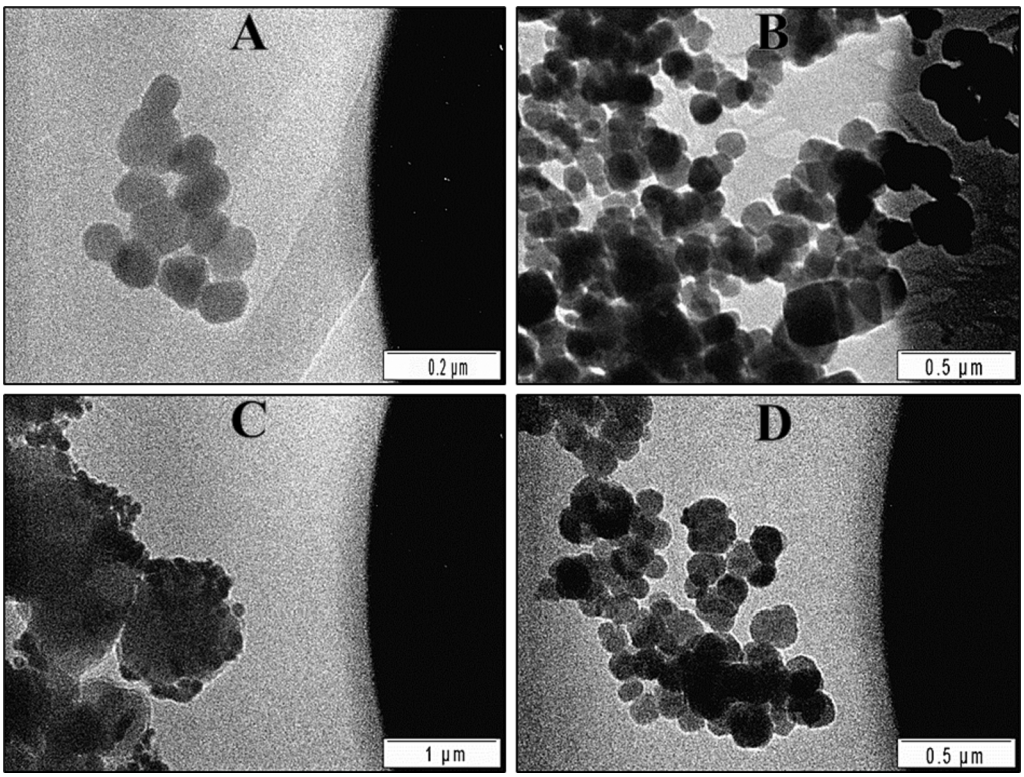

Fig. 3. TEM images of IONP's (A), PEI-IONPs (B), Au(seed) PEI-IONP's (C) and Au-IONP's (D).

another source of steric hindrance. The 4-carbon linker may be less affected by both of these scenarios by having fewer rotatable bonds in the chain length than TTLD6, but still long enough to be less affected by steric hindrance than TTLD3.

3.8. Stability study of the TTLD-(Au-IONP) formulation at 20 °C

Prior to heating, the drug loaded Au-IONP's were magnetically separated, and the supernatant was sampled for a T = 0 min time point. At 20 °C, the release of TTLD4 and TTLD6 over the 180 min period was less than 1%, as shown in Fig. 5. This suggests that negligible amount of the retro Diels-Alder reaction was taking place over the 3 h period and that they are stable without additional heating.

Approximately 12% of TTLD3 was released over 180 min at 20 °C, the majority of which occurred within two minutes. The amount of TTLD detected decreased between time points at the 2-min and 15-min time point, suggesting a form of reattachment of the whole linker to the Au-IONP surface, rather than a breakdown via retro Diels-Alder. After 30 min, the change in release rate is negligible, and similar to TTLD4 and TTLD6, indicating that the original release was probably due to thiolated conjugates which had not properly attached onto the Au-IONP and were held within the bound conjugates, but once these were liberated, that formulation stability was consistent, without the input of heat.

3.9. TTLD-(Au-IONP) formulation drug release at 37, 45 and 60 °C

There is an initial "burst release" that occurs between within 30 min for all three linker analogues as shown in Fig. 6 where all three linkers are confirmed to be temperature sensitive at 37 °C, 45 °C and 60 °C, with the release rate increasing at higher temperatures. Secondly, there is a correlation between linker length and release rate, where decreasing linker length promotes faster drug release.

There is a large and consistently rapid release of all 3 linkers that occurs exponentially within the first 30 min at 45 °C. Approximately 93.6% of TTLD3 was released after 180 min, compared to 75.9% and 48.5% for TTLD4 and TTLD6, respectively. This confirms the correlation of shorter linker lengths leading to faster rates of drug release, where TTLD3 undergoes retro Diels-Alder mediated release 23% and 93% faster than TTLD4 and TTLD6, respectively. It is worth noting that TTLD3 also had approximately 3-fold less loading that TTLD4 and 2-fold less than TTLD6. Therefore, in terms of relative drug release, the TTLD4-(Au-IONP) formulation released approximately 2.5-fold more drug-linker by mass than the TTLD3 formulation. Secondly, the TTLD6-(Au-IONP) formulation had 2.24 times more drug loaded compared to the TTLD3-(Au-IONP) and subsequently released 16% more drug by mass over 180 min.

The "burst release" of the TTLD linkers is higher at 60 ℃ than at 45 and 37 ℃ within the first 30 min. The difference in overall % drug release at 60 °C however is lower after 180 min when compared to the 45 C data, as all three formulations have surpassed 80 % total release by this point, with shorter linker lengths contributing more to more overall drug release.

This study expands on previously established research regarding reversibly bound gemcitabine onto the surface of Au-IONP's via a Diels-Alder cycloadduct linker as a potential treatment for pancreatic cancer, by modification of the Diels-Alder linker length. We report a clear correlation between the linker length and its effect on the rate of drug release, wherein shorter linkers undergo retro Diels-Alder mediated release at a faster rate. Drug loading was highest for TTLD4 (76%), followed by TTLD6 (57%) with the lowest loading for TTLD3 (25%). The innate chemical inertness of gold and the ease of which the gold-thiol bond forms suggests that the difference is due to physical restrictions such as steric hinderance caused by a combination of the terminal gemcitabine group being closer to the surface which would impact TTLD3 the most, and/or the longer alkyl chain length of the Diels-Alder linker facilitating a more horizontal positioning on the Au-IONP surface, which would occur with TTLD6 more frequently. Therefore, TTLD4 may merely benefit from a reduction in both factors that inhibit drug loading. Additionally, the bond angle arrangement of the alkyl bonds in the linkers containing an even number of linker carbons, such as in TTLD4

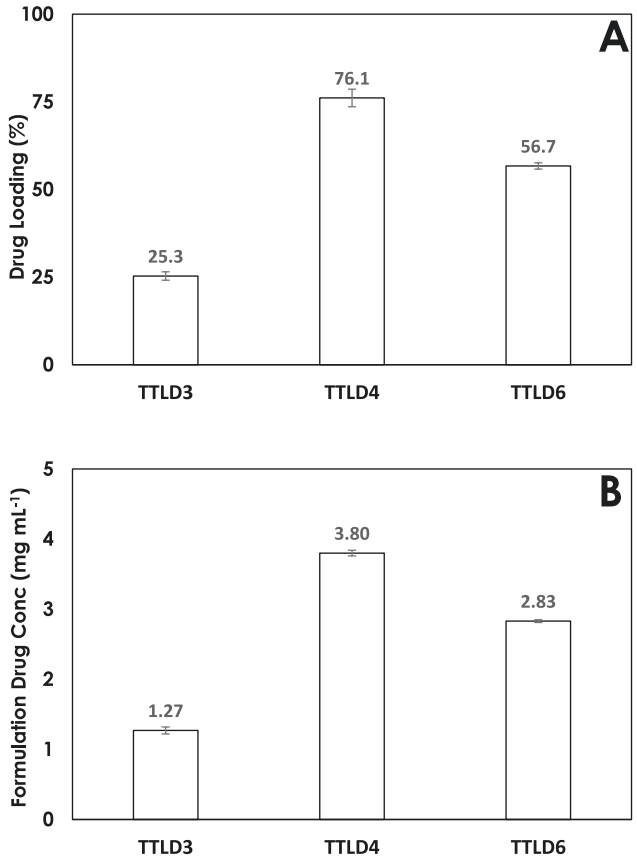

Fig. 4. (A) Bar chart of the % loading of drugs on Au-IONP's at a ratio of 5:1 Drug/Au-IONP, (B) and the concentration (mg mL^{-1}) of loaded drugs on Au-IONP's for all three TTLD analogues determined by HPLC (B).

and TTLD6, leads to a structure that that may extend perpendicular to the Au-IONP surface. An odd number of linker carbons in TTLD3 could lead to a staggered orientation from the surface that might block some binding sites. This is illustrated in Fig. 1 where TTLD3 is not perpendicular to the Au-IONP surface. Future work involving the conjugation of a TTLD5 analogue would confirm if this odd-number rule is true. The drug release studies which were performed over 180 min, demonstrated that approximately half of the overall drug release occurred within the first 5 min, in which 60%, 52% and 28% was released for TTLD3, TTLD4 and TTLD6, respectively, thus demonstrating the rapid retro Diels-Alder mediated "burst release" behaviour of the linkers within minutes at elevated temperatures. This is important for subsequent *in vivo* studies where sufficient drug release must occur with only a short exposure time to near infra-red laser light. These results highlight the possibility of designing formulations containing a blend of linkers to treat pancreatic cancer. A blend of the linkers would enable the creation of formulations with finely tuned release rates. A higher proportion of TTLD3 would suit formulations designed for rapid release, while increasing TTLD6 content would function as a method of smoothing out release profiles. This may enable secondary "burst release" events when elevated temperatures are applied a second time. Current chemotherapeutic practices usually involve the repeated administration of anti-cancer agents such as gemcitabine or capecitabine. Drug loaded Au-IONP's containing multiple doses could benefit from a TTLD blend that enabled repeated burst release windows. The combination first line treatment of pancreatic cancer is a drug formulation called GemCap given in 28-day cycles, in which gemcitabine is typically administered weekly over 30 min intravenously for three weeks and capecitabine is administered orally twice a day for 21 days. The side effects of GemCap are more severe than gemcitabine alone and this may prevent the use of GemCap on some pancreatic cancer patients due to their advanced age and likely comorbidities. It should be noted that capecitabine is a pro-drug and requires metabolism to give the active 5-fluorouracil (5-FU). The requirement for liver metabolism of capecitabine and the ability of gemcitabine to accumulate within the tumour environment varies from patient to patient. As such, no two patient's intratumor drug uptake and subsequent activity is identical. The surface conjugation of 5-

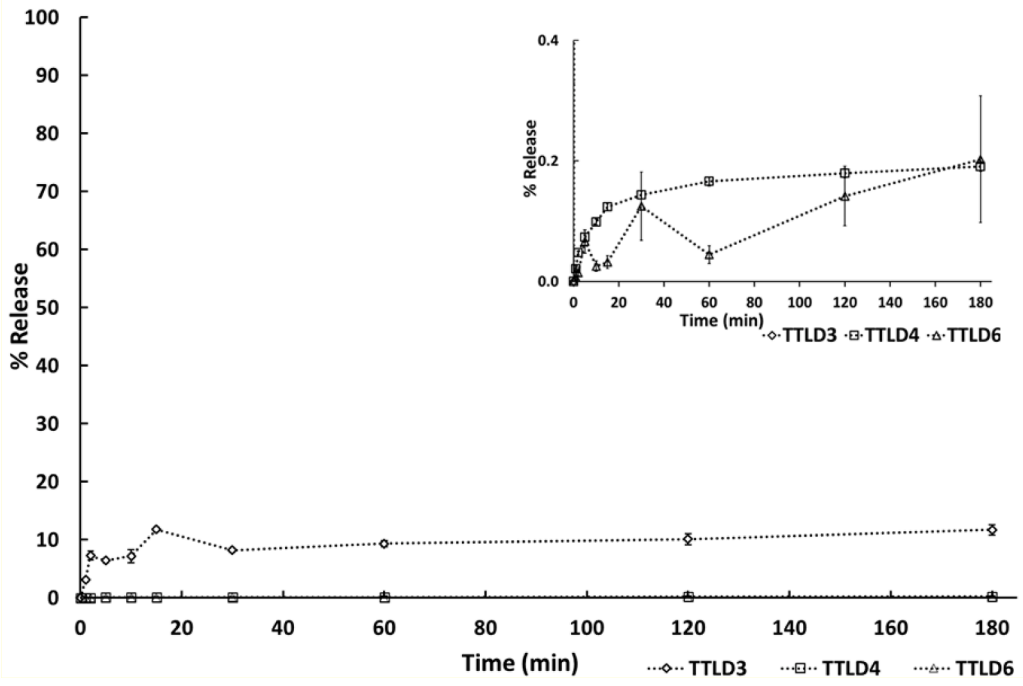

Fig. 5. (A) Graph for the release of TTLD3, TTLD4 and TTLD6 at 20 °C and (B) a subgraph focused on scaled to 0.4% release. Error bars were calculated using the standard deviation of n = 3 results.

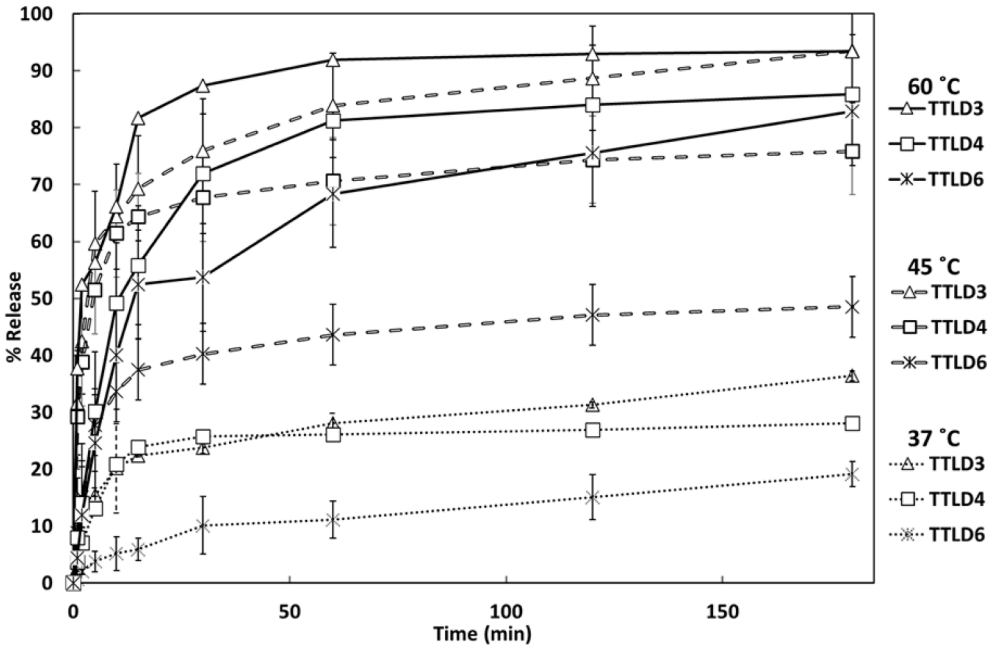

Fig. 6. Graph for the retro Diels-Alder mediated release of TTLD3, TTLD4 and TTLD6 from the Au-IONP surface at 37, 45 and 60 °C.

fluorouracil alongside gemcitabine onto the surface of Au-IONP's would enable the local controlled release of a conceptual equivalent of Gem-Cap. The ratio of each drug's respective release could be enabled with the use of different linker blends.

4. Conclusion

The differences in the release of gemcitabine, based on variations in TTLD-(Au-IONP) linker length offer additional opportunities to further control the overall retro Diels-Alder mediated release of gemcitabine from Au-IONP surfaces. This includes the possibility of generating TTLD-(Au-IONP) formulations comprising of further lengthened TTLD linkers to fine tune the retro Diels-Alder mediated release, which would allow a greater picture of the general trends. This study can be expanded upon with the synthesis and evaluation of additional linkers, particularly those containing an odd number of linker carbons to evaluate the odd vs even theory for drug loading. Linkers exceeding the 6-carbon length could also be synthesised to further confirm the relationship between linker length and drug release. Furthermore, this would extend to linkers of significant length containing hundreds to thousands of carbons. Lastly, in vitro studies would also be implemented to determine the cellular uptake rate of these linkers. All three linkers within this study, demonstrated the typical burst release profile where half of the total release that occurred over the first 3 h, took place within the first 5 min with the use of thermal blocks. Future applications where the different release rates of the TTLD linkers will be exploited with the use of laser or magnetically induced heating which is more in line with potential clinical use. This highlights the possibility of introducing sequential heat-mediated release of conjugated materials within the tumour environment for treating pancreatic cancer.

CRediT authorship contribution statement

Adeolu Oluwasanmi: Data curation, Methodology, Writing – original draft. **Sarah Lindsay:** Methodology, Data curation. **Anthony Curtis:** Methodology, Data curation. **Yvonne Perrie:** Supervision. **Clare Hoskins:** Conceptualization, Supervision.

Declaration of Competing Interest

The authors declare that they have no known competing financial interests or personal relationships that could have appeared to influence the work reported in this paper.

Data availability

Data will be made available on request.

Appendix A. Supplementary material

Supplementary data to this article can be found online at https://doi.org/10.1016/j.ijpharm.2023.123304.

References

Bachem, M.G., et al., 2005. Pancreatic carcinoma cells induce fibrosis by stimulating proliferation and matrix synthesis of stellate cells. Gastroenterology 128, 907–921. https://doi.org/10.1053/J.GASTRO.2004.12.036.

Barnett, C.M., et al., 2012a. Effect of the hybrid composition on the physicochemical properties and morphology of iron oxide-gold nanoparticles. J. Nanopart. Res. 14, 1170. https://doi.org/10.1007/s11051-012-1170-4.

Barnett, C.M., et al., 2012b. Effect of the hybrid composition on the physicochemical properties and morphology of iron oxide-gold nanoparticles. J. Nanopart. Res. 14, 1–12. https://doi.org/10.1007/S11051-012-1170-4/FIGURES/7.

Barnett, C.M., et al., 2013. Physical stability, biocompatibility and potential use of hybrid iron oxide-gold nanoparticles as drug carriers. J. Nanopart. Res. 15 https://doi.org/10.1007/s11051-013-1706-2.

Borsenberger, V., Howorka, S., 2009. Diene-modified nucleotides for the Diels-Alder-mediated functional tagging of DNA. Nucl. Acids Res. 37, 1477–1485. https://doi.org/10.1093/nar/gkn1066.

Boutelle, R.C., Northrop, B.H., 2011. Substituent effects on the reversibility of furan-maleimide cycloadditions. J. Org. Chem. 76, 7994–8002. https://doi.org/10.1021/jo201606z.

Breast cancer survival statistics | Cancer Research UK. <https://www.cancerresearchuk.org/health-professional/cancer-statistics/statistics-by-cancer-type/breast-cancer/survival#heading-Two> (Accessed 6.29.22).

Brooks, J.R., Culebras, J.M., 1976. Cancer of the pancreas: palliative operation, whipple procedure, or total pancreatectomy? Am. J. Surg. 131, 516–520. https://doi.org/10.1016/0002-9610(76)90167-7.

Burris, H.A., et al., 1997. Improvements in survival and clinical benefit with gemcitabine as first-line therapy for patients with advanced pancreas cancer: a randomized trial. J. Clin. Oncol. 15, 2403–2413. https://doi.org/10.1200/JCO.1997.15.6.2403.

Changazi, S.H., et al., 2020. Whipple procedure: a five-year clinical experience in tertiary care center. Cureus 12, 11466. https://doi.org/10.7759/cureus.11466.

Conroy, T., et al., 2018. FOLFIRINOX or gemcitabine as adjuvant therapy for pancreatic cancer. N. Engl. J. Med. 379, 2395–2406. https://doi.org/10.1056/NEJMoa1809775.
de Jong, E.J.M., et al., 2022. Real-world evidence of adjuvant gemcitabine plus capecitabine vs gemcitabine monotherapy for pancreatic ductal adenocarcinoma. Int. J. Cancer 150, 1654–1663. https://doi.org/10.1002/ijc.33916.
Diels, O., Alder, K., 1929. Synthesen in der hydro-aromatischen Reihe, II. Mitteilung: Über Cantharidin. Bericht. deutschen chemischen Gesellschaft (A and B Ser.) 62, 554–562. https://doi.org/10.1002/cber.19290620318.
Guo, Z.-W., Gallo, J.M., 1999. Selective Protection of 2′,2′-Difluorodeoxycytidine (Gemcitabine). J. Org. Chem. 64, 8319–8322. https://doi.org/10.1021/jo9911140.
Herrmann, R., et al., 2007. Gemcitabine plus capecitabine compared with gemcitabine alone in advanced pancreatic cancer: a randomized, multicenter, phase III trial of the Swiss Group for Clinical Cancer Research and the Central European Cooperative Oncology Group. J. Clin. Oncol. 25, 2212–2217. https://doi.org/10.1200/JCO.2006.09.0886.
Hoskins, C., et al., 2012. Hybrid gold-iron oxide nanoparticles as a multifunctional platform for biomedical application. J Nanobiotechnology 10, 1–12. https://doi.org/10.1186/1477-3155-10-27/FIGURES/7.
Houk, K.N., et al., 1986. Evidence for the concerted mechanism of the Diels-Alder reaction of butadiene with ethylene. J. Am. Chem. Soc. 108, 554–556. https://doi.org/10.1021/ja00263a059.
Jameson, G.S., et al., 2020. Response rate following albumin-bound paclitaxel plus gemcitabine plus cisplatin treatment among patients with advanced pancreatic cancer a phase 1b/2 Pilot clinical trial supplemental content. JAMA Oncol. 6, 125–132. https://doi.org/10.1001/jamaoncol.2019.3394.
Karagiannis, G.S., et al., 2012. Cancer-associated fibroblasts drive the progression of metastasis through both paracrine and mechanical pressure on cancer tissue. Mol. Cancer Res. 10, 1403–1418. https://doi.org/10.1158/1541-7786.MCR-12-0307.
Karamitopoulou, E., 2019. Tumour microenvironment of pancreatic cancer: immune landscape is dictated by molecular and histopathological features. Br. J. Cancer 121, 5–14. https://doi.org/10.1038/s41416-019-0479-5.
Kolb, H.C., et al., 2001. Click chemistry: diverse chemical function from a few good reactions. Angew. Chem. Int. Ed. 40, 2004–2021. https://doi.org/10.1002/1521-3773(20010601)40:11<2004::AID-ANIE2004>3.0.CO;2-5.
Konstantinidis, I.T., et al., 2013. Pancreatic ductal adenocarcinoma: Is there a survival difference for R1 resections versus locally advanced unresectable tumors? What is a "true" R0 resection? Ann. Surg. 257, 731–736. https://doi.org/10.1097/SLA.0B013E318263DA2F.
Latenstein, A.E.J., et al., 2020. Nationwide trends in incidence, treatment and survival of pancreatic ductal adenocarcinoma. Eur. J. Cancer 125, 83–93. https://doi.org/10.1016/J.EJCA.2019.11.002.
Nießen, A., Hackert, T., 2021. State-of-the-art surgery for pancreatic cancer. Langenbecks Arch. Surg. 407, 443–450. https://doi.org/10.1007/s00423-021-02362-y.
O'Reilly, E.M., et al., 2020. Randomized, multicenter, phase II trial of gemcitabine and cisplatin with or without Veliparib in patients with pancreas adenocarcinoma and a germline BRCA/ PALB2 mutation. J. Clin. Oncol. 38, 1378–1388. https://doi.org/10.1200/JCO.19.
Oluwasanmi, A., et al., 2017. Diels Alder-mediated release of gemcitabine from hybrid nanoparticles for enhanced pancreatic cancer therapy. J. Control. Release 266. https://doi.org/10.1016/j.jconrel.2017.09.027.
Ottaviano, A.J., et al., 2006. Extracellular matrix-mediated membrane-type 1 matrix metalloproteinase expression in pancreatic ductal cells is regulated by transforming growth factor-B1. Cancer Res. 66, 7032–7072. https://doi.org/10.1158/0008-5472.CAN-05-4421.
Pancreatic cancer survival statistics | Cancer Research UK. <https://www.cancerresearchuk.org/health-professional/cancer-statistics/statistics-by-cancer-type/pancreatic-cancer/survival#heading-Two> (Accessed 6.29.22).
Peters, G.J., et al., 2007. Clinical phase I and pharmacology study of gemcitabine (2', 2'-Difluorodeoxycytidine) administered in a two-weekly schedule. J. Chemother. 19, 212–221. https://doi.org/10.1179/joc.2007.19.2.212.
Qiu, Y., 2015. Substituent effects in the Diels-Alder reactions of butadienes, cyclopentadienes, furans and pyroles with maleic anhydride. J. Phys. Org. Chem. 28, 370–376. https://doi.org/10.1002/poc.3421.
Rickborn, B., 1998. The Retro-Diels-Alder Reaction Part II. Dienophiles with One or More Heteroatom, in: Organic Reactions. John Wiley & Sons, Inc., Hoboken, NJ, USA, pp. 223–629. <https://doi.org/10.1002/0471264180.or053.02>.
Song, H.Y., et al., 2009. Practical synthesis of maleimides and coumarin-linked probes for protein and antibody labelling via reduction of native disulfides †. Org. Biomol. Chem. 7, 3400–3406. https://doi.org/10.1039/b904060a.
Temperini, A., et al., 2010. A simple acylation of thiols with anhydrides. Tetrahedron Lett. 51, 5368–5371. https://doi.org/10.1016/J.TETLET.2010.07.126.
von Hoff, D.D., et al., 2013. Increased survival in pancreatic cancer with nab-paclitaxel plus gemcitabine. NEJM.org N. Engl. J. Med. 18, 1691–1703. https://doi.org/10.1056/NEJMoa1304369.
Vreeland, T.J., et al., 2019. Benefit of gemcitabine/nab-paclitaxel rescue of patients with borderline resectable or locally advanced pancreatic adenocarcinoma after early failure of FOLFIRINOX HHS public access. Pancreas 48, 837–843. https://doi.org/10.1097/MPA.0000000000001345.
Xie, Y., et al., 2020. Stromal modulation and treatment of metastatic pancreatic cancer with local intraperitoneal triple miRNA/siRNA nanotherapy HHS public access. ACS Nano 14, 255–271. https://doi.org/10.1021/acsnano.9b03978.
Yang, W., Huang, J., et al., 2021. Shape effects of gold nanoparticles in photothermal cancer therapy. Mater. Today Sust. 13, 100078 https://doi.org/10.1016/J.MTSUST.2021.100078.
Zhang, Y., et al., 2019. Nab-paclitaxel plus gemcitabine as first-line treatment for advanced pancreatic cancer: a systematic review and meta-analysis. J. Cancer 10, 4420–4429. https://doi.org/10.7150/jca.29898.
Zhou, J., Guimard, et al., 2012. Thermally reversible Diels-Alder-based polymerization: an experimental and theoretical assessment. Polym. Chem. 3, 628–639. https://doi.org/10.1039/c1py00356a.